

Journal of Materials Chemistry A

Characterization of Pitch Carbon Coating Properties Affecting the Electrochemical Behavior of Silicon Nanoparticle Lithium-ion Battery Anodes

Journal:	Journal of Materials Chemistry A	
Manuscript ID	TA-ART-06-2024-004478.R1	
Article Type:	Paper	
Date Submitted by the Author:	1 /5-San- /11/4	
Complete List of Authors:	Huey, Zoey; National Renewable Energy Laboratory, ; Colorado School of Mines, Schulze, Maxwell; National Renewable Energy Laboratory Carroll, G.; National Renewable Energy Laboratory, Chemistry and Nanoscience Engtrakul, Chaiwat; National Renewable Energy Laboratory Jiang, Chun-Sheng; National Renewable Energy Laboratory DeCaluwe, Steven; Colorado School of Mines, Mechanical Engineering Tremolet de Villers, Bertrand; National Renewable Energy Laboratory, Chemistry and NanoScience Center Han, Sang-Don; Sejong University, Chemistry Department	

SCHOLARONE™ Manuscripts

Characterization of Pitch Carbon Coating Properties Affecting the Electrochemical Behavior of Silicon Nanoparticle Lithium-ion Battery Anodes

Zoey Huey, ^{a,b} Maxwell C. Schulze, ^a G. Michael Carroll, ^a Chaiwat Engtrakul, ^a Chun-Sheng Jiang, ^a Steven C. DeCaluwe, ^b Bertrand J. Tremolet de Villers, ^{a,*} and Sang-Don Han^{a,c,*}

- ^a Materials, Chemical, and Computational Science Directorate, National Renewable Energy Laboratory, Golden, Colorado 80401, United States
- ^b Department of Mechanical Engineering, Colorado School of Mines, Golden, Colorado 80401, United States
- ^c Department of Chemistry, Sejong University, Seoul, 05006, Republic of Korea

E-mails: shan@sejong.ac.kr, bertrand.tremolet@nrel.gov

Keywords: pitch-coated silicon nanoparticle, solid-electrolyte interphase, surface chemistry, electronic resistivity, heterogeneous aging behavior

Abstract

Silicon is an exciting material for next-generation lithium-ion battery anodes, due to its high theoretical capacity and availability, but its widespread implementation has been limited by extensive volume changes during cycling that causes mechanical damage and limits cycle life. One approach to mitigating these deleterious effects while still maintaining silicon's benefits is the addition of a pitch carbon coating to nanometer-sized silicon particles. Here, we present characterization of pitch-coated silicon electrodes without annealing and annealed at 700 °C and 1000 °C to determine the optimum temperature treatment, as well as pitch-only and silicon-only electrodes with and without annealing to elucidate the impacts of each component on early electrochemical behavior. Using Fourier transform infrared and Raman spectroscopies, atomic force and scanning spreading resistance microscopies, and electrochemical analysis, we find 700 °C to be the optimal annealing temperature, as amorphous carbon is created, which improves conductivity prior to cycling and facilitates ion storage during cycling that increases capacity. We also present in-situ Raman spectroscopy data demonstrating the heterogeneous aging that occurs across the electrode surface during cycling.

1. Introduction

As the decarbonization of global energy sectors accelerates, there is an increasing need for higher capacity energy storage devices for applications such as electric vehicles. Silicon (Si) has a much greater theoretical capacity (3579 mAh g⁻¹) than the current standard graphite anode material (372 mAh g⁻¹) in lithium ion batteries (LiBs), making it a promising material for next-generation anodes [1]. However, Si expands and contracts dramatically during cycling (lithiation/delithiation), which poses mechanical issues as well as creates an unstable solid electrolyte interphase (SEI) [2, 3]. As Si is cycled, cracks form during its expansion, exposing fresh Si to electrolyte, which accelerates electrolyte decomposition and reduces cycle life [4].

Several strategies have been explored to overcome these challenges while still benefiting from Si's high capacity, including coating the Si particles in composite anodes with various materials to mitigate the expansion of Si and prevent reactivity by providing a barrier between the Si and electrolyte [5, 6]. Types of coatings studied so far include metals, metal oxides, silicon oxides, and various forms of carbon and graphite [7, 8]. Carbon is both inexpensive and electronically conductive, making it a practical and beneficial coating material [9]. Petroleum pitch carbon in particular is a readily available industrial by-product, making it a convenient and practical material for coating Si and improving anode performance [10, 11].

Typically, pitch-coated Si electrodes undergo some type of heat treatment during manufacturing, although temperatures and processes utilized in the literature vary [9, 10, 12]. This heating improves performance because it transforms the pitch into amorphous carbon, or even graphite if the temperature is high enough (> 2000 °C). Amorphous carbon and graphite improve cell performance due to increased conductivity and increased capacity due to improved Li⁺ ion storage [13, 14]. Disordered carbon, such as that extracted from petroleum pitch, can adsorb ions

onto its surface and then accumulate them in pores and three-dimensional structures with partial ion insertion into the structure. Conversely, graphitic carbon stores Li⁺ ions via intercalation between its constituent graphene sheets, forming LiC₆ [15, 16]. These differing ion storage mechanisms result in different electrochemical voltage profiles and a lower energy density in non-graphitic carbon [17]. Thus, increasing the graphitic nature of the pitch in anodes is desirable to improve cycling performance.

Using multiple characterization techniques, this work examines optimal annealing temperature for electrodes made with pitch-coated Si (Si/pitch) nanoparticles (5.9 nm diam.), the impacts of annealing on the physical properties of the electrode materials, and how annealing impacts SEI formation and evolution and overall electrochemical behavior [11, 18].

2. Results and Discussion

2.1. Characterization of Si/pitch electrodes

2.1.1. Surface chemistry and structure changes

Fourier-transform infrared (FTIR) and Raman spectroscopy were used to characterize the chemical changes of Si/pitch electrodes, specifically focusing on their individual components and structural changes after heat treatments. A composite electrode consisting of petroleum pitch carbon (extracted by toluene solvent fractionation), conductive carbon (Super C65, TIMCAL), and polyimide binder (P84, Ensinger Plastics) was slurry cast from n-methyl pyrrolidone (NMP) solvent onto a copper foil and dried at 120 °C, resulting in a composite film with mass ratio of 80:10:10 pitch carbon:C65:P84. An attenuated total reflectance (ATR)-FTIR spectrum of the electrode (Fig. 1a, black trace) shows that the electrode composite signal is a combination of the spectral features of its individual components: pitch carbon powder (red trace), conductive carbon

(green trace) and P84 binder (blue trace). Therefore, ATR-FTIR can be used to identify changes in the individual components of the electrode during a heat treatment. Chemical changes of pitch carbon due to thermal treatment at 700 °C or 1000 °C were then characterized. In the ATR-FTIR spectra of pitch carbon electrodes (Fig. 1b), it can be seen that after heating, there is a loss of certain peaks, specifically around 1580 cm⁻¹ and 1350 cm⁻¹ and also between 900-800 cm⁻¹, that are associated with -CH_x vibrational modes. This peak loss suggests that heat treatments result in a loss of aliphatic groups, indicating a less substituted pitch carbon with more poly-aromatic hydrocarbon (PAH) character [19].

Si-based pitch-containing electrodes were made by first combining nano-Si made by plasmenhanced chemical vapor deposition (PECVD) with pitch carbon in a toluene solution, drying, then carbonizing the Si powder at either 700 °C or 1000 °C. A non-heated mixture was made as a control as well. The carbon-coated Si was then used to make a slurry in NMP which was subsequently cast onto a copper foil and dried at 120 °C to make an electrode with a final mass composition ratio of 80% Si/pitch (50:50), 10% Super C65 conductive carbon, and 10% P84 binder. These electrodes then underwent a curing process at 400 °C which is known to improve performance due to the removal of surface atoms [18]. Fig. 1c shows the ATR-FTIR spectra of the three Si/pitch electrodes. The electrode using unheated Si/pitch electrode (Si/pitch-U, black trace) shows an intense broad peak between 1200-900 cm⁻¹, attributed to silicon (SiO_x) in the film [20]. Peak characteristics of the pitch carbon are also observed below 900 cm⁻¹. The electrode using Si/pitch heated to 700 °C (Si/pitch-700) has a significantly different ATR-FTIR spectrum (red trace) compared to the electrode with unheated Si/pitch. The silicon peak between 1200-900 cm⁻¹ is greatly diminished. This is likely because most of the Si nanocrystals are covered by the pitch carbon after the heating step. So instead of detecting the Si, FTIR reveals mostly signal from

the pitch carbon, below 900 cm⁻¹. However, this shape of the broad peak in this region is different from the one with the electrode with unheated Si/pitch. Consistent with the observations from Fig. 1b, the 700 °C pitch carbon has lost much of its aliphatic carbon signal between 900-800 cm⁻¹.

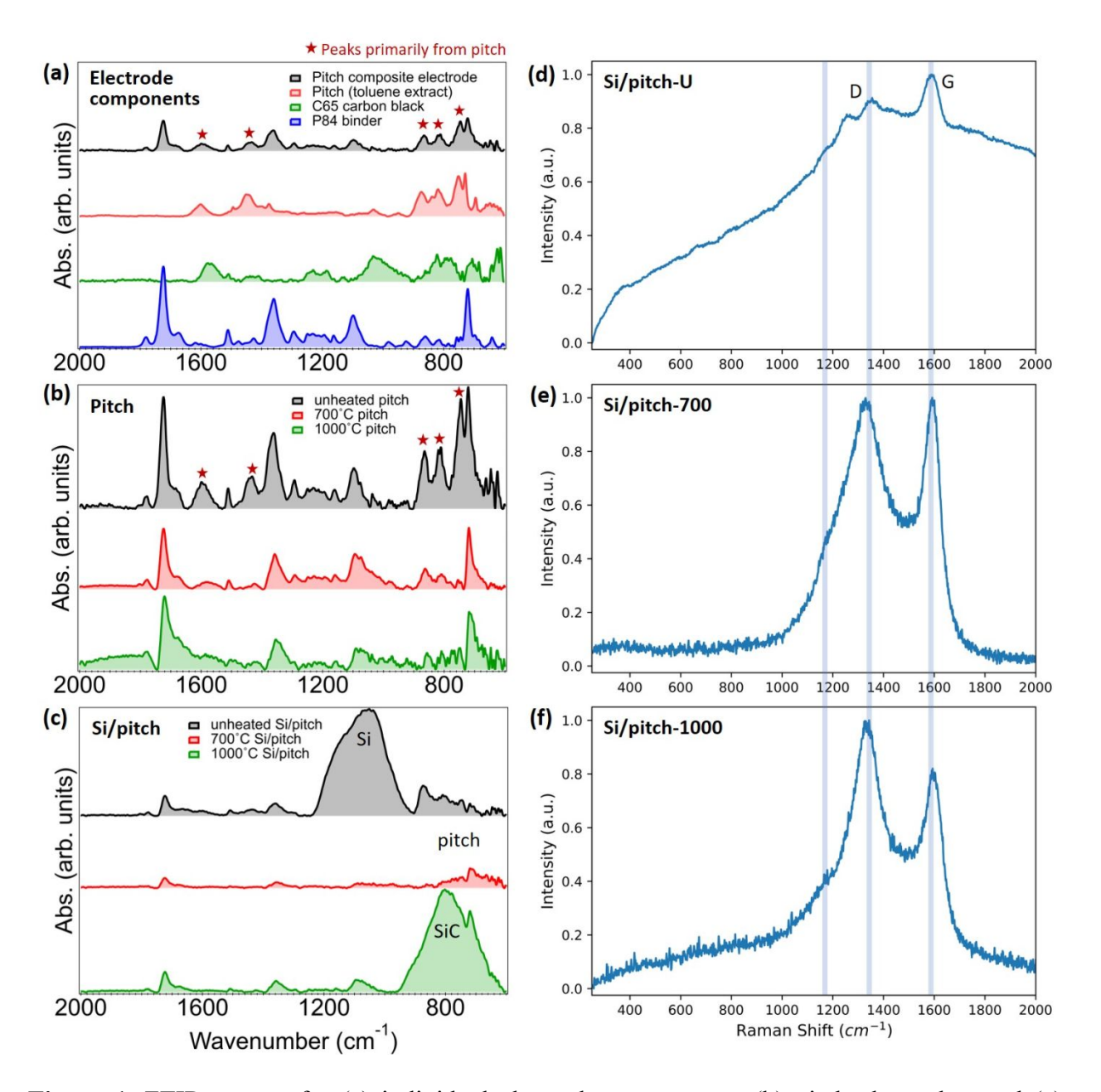


Figure 1. FTIR spectra for (a) individual electrode components, (b) pitch electrodes, and (c) Si/pitch electrodes during annealing at different temperatures. (d-f) Raman scattering results demonstrating effect of heat treatment on Si/pitch electrodes.

In contrast to the other Si electrodes, the electrode using Si/pitch annealed to 1000 °C (Si/pitch-1000) is dominated by an intense peak around 800 cm⁻¹ (green trace in Fig. 1c). This is a well-known peak for silicon carbide (Si-C), and indicates that heating the silicon/pitch powder mixture much above 700 °C results in a chemical reaction between the silicon and carbon to form Si-C [21]. To confirm the formation of Si-C above 700 °C, we have also measured the X-ray diffraction patterns of our Si/pitch powders (Fig. S1): the unheated and 700 °C Si/pitch match our previously published XRD data for our PECVD Si nanocrystals with prominent 2-theta peaks at 28.71°, 47.62°, and 56.45° for [111], [220], and [311] reflection planes, respectively [22], and the 1000 °C Si/pitch sample instead shows the diffraction pattern characteristic of Si-C with these peaks shifted to 35.81°, 60.30°, and 71.9°, respectively [23]. In terms of a lithium-ion battery material, Si-C requires complex engineering design to benefit an electrode, as it can have low ionic and electronic conductivity and can instead act as a barrier to storing charge in the anode [24, 25].

To delve deeper into the changes of the pitch carbon with heat treatment, Raman scattering was used to characterize the three different Si/pitch electrodes. The Raman spectra between 300-2000 cm⁻¹ are shown in Figure 1d-f for electrodes using unheated Si/pitch, 700°C heated Si/pitch and 1000°C heated Si/pitch, respectively. With no heat treatment, the Si/pitch electrode Raman spectrum is dominated by the highly fluorescent pitch carbon [26]. In contrast, the heat-treated electrodes both show prominent Raman bands at 1380 and 1590 cm⁻¹. These bands are commonly labeled as D and G bands, respectively [27, 28]. For graphite (with high crystallinity), the G band has a high intensity and small (<50 cm⁻¹) full width at half maximum (FWHM), while the D band intensity is almost zero. The two Raman bands for the heated treated electrodes have relatively equal intensity indicating an amorphous carbon structure [27]. These data agree with FTIR where increasing the annealing temperature facilitates the formation of amorphous carbon (and loss of

aliphatic carbon) with sp² and sp³ carbon. Heating up to 1000°C further carbonizes the pitch (more sp² carbon) leading to a decrease in FWHM, increase in D band peak intensity to G band peak intensity ratio, and red shift of the D band. [27, 28].

2.1.2. Electronic resistivity and morphology

Scanning Spreading Resistance Microscopy (SSRM) imaging is a scanning-probe based technique that measures localized material resistivity with a depth sensitivity less than 50 nm and provides more detailed electronic property measurements than other techniques such as a four point probe measurement or electrochemical impedance spectroscopy [29]. SSRM data demonstrates the surface of electrodes made with only pitch showed a decrease in resistivity from annealing that is greater at 1000 °C than 700 °C (Fig. 2a) [30, 31]. For Si/pitch composite anodes, the different resistivities of the electrode components (e.g., Si, pitch carbon, conductive carbon and polyimide binder) allows direct identification resistivity (Fig. S2) and previous study [32]. While the resistivity values of pitch and amorphous carbon can vary significantly due to factors such as defects, impurities, crystallinity, orientation, and powder compaction, literature reports that as carbon becomes more ordered at higher treatment temperatures, resistivity decreases [33-36].

Si/pitch electrodes also show a decrease in resistivity after heat treatment, although the resistivity is similar at 700 °C and 1000 °C (Fig. 2b). These results indicate that a resistivity decrease in the Si/pitch-700 electrodes is driven by the pitch carbonization, while the resistivity decrease in the Si/pitch-1000 electrodes is inhibited by the Si, resulting in a similar resistivity to the Si/pitch-700 electrode. These results are consistent with the FTIR and Raman data showing the shift from pitch to disordered hard carbon during annealing, as well as the formation of SiC at 1000 °C [37].

Electrodes made with only Si and P84 were measured with no heat treatment and after the curing step at 400°C and showed no change in individual component resistivity (e.g., Si and binder), as shown in Fig. 2c. Due to the high intrinsic resistivity of Si, it is common to incorporate some type of conductive component to Si electrodes to promote Si utilization and improve capacity [38, 39]. It is likely that the decrease in resistivity observed here is correlated to improved cycling capacity demonstrated later in this work.

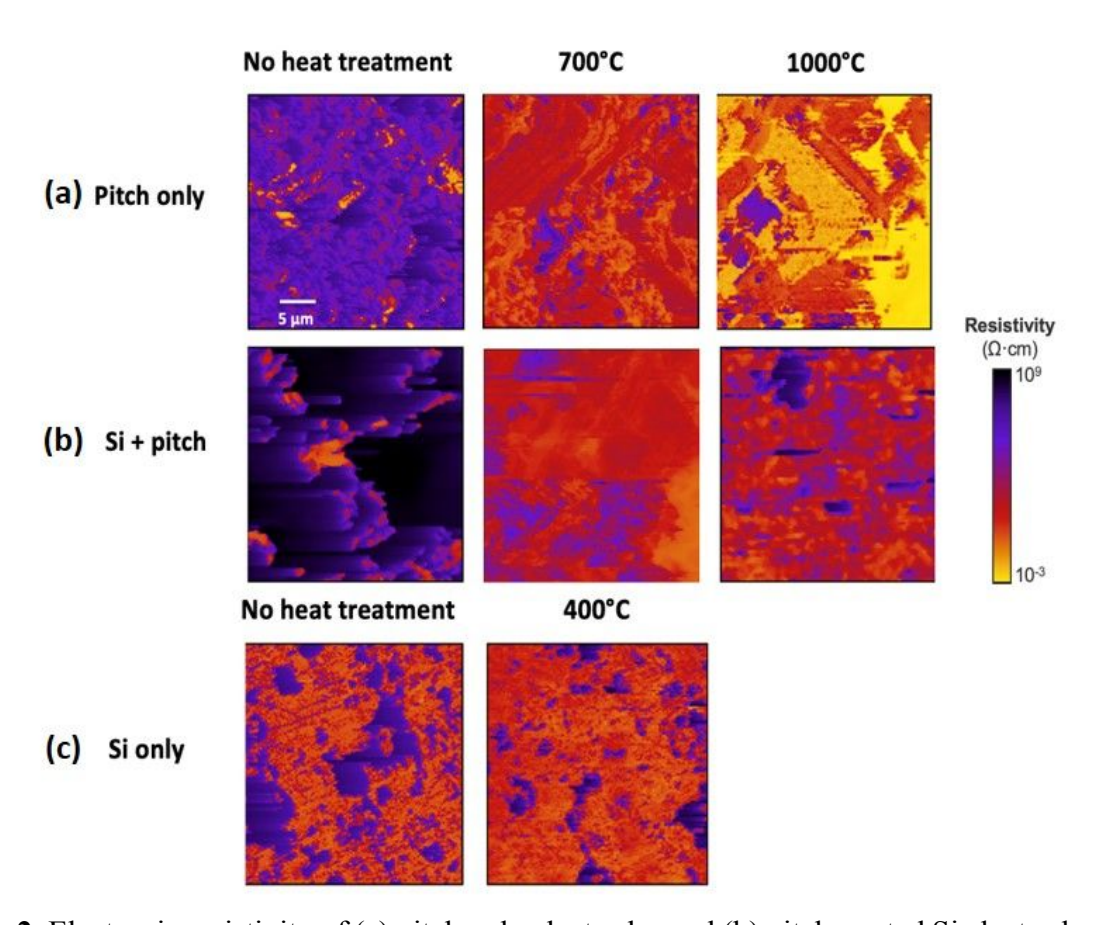


Figure 2. Electronic resistivity of (a) pitch only electrodes and (b) pitch-coated Si electrodes upon thermal annealing and (c) Si only electrodes (with *vs.* without heat treatment).

We collected atomic force microscopy (AFM) surface maps to analyze the roughness and morphology of the pristine pitch-only electrode surfaces, as shown in Fig. S3. The unannealed pitch electrodes (pitch-U) and pitch electrodes annealed at 700 °C (pitch-700) have similar

morphologies, with visible particles around 1 μ m in diameter. The pitch electrodes annealed at 1000 °C (pitch-1000) have much larger features, with visible particles of 5 μ m or larger, and higher surface roughness. This change in feature size may indicate a morphology change that occurs along with the shift from pitch to amorphous carbon that occurs during annealing.

2.2. Electrochemistry of Si/pitch electrodes

To verify the electrochemical contributions of the pitch-carbon coating, electrodes with only pitch and Si/pitch electrodes were cycled and their electrochemical behaviors and performance were compared. Pitch-only electrodes, shown in Figs. 3a and 3b, show observable capacities. Additionally, both pitch-700 and pitch-1000 electrodes show notably different voltage profiles (Fig. 3a) and corresponding differential capacity curves (inset of Fig. S4a) when compared to the pitch-U. These indicate severe electrolyte decomposition and SEI formation due to increased surface area after the heat treatment, and possibly different ionic storage mechanisms due to the structural changes observed in the pitch-carbon. The unannealed pitch is only able to adsorb limited amounts of Li⁺ ions on its surface, which restricts capacity. When annealed, the pitch transforms into mostly amorphous carbon, but with some regions of graphitic character that can also store Li⁺ ions within its lattice via insertion as well as adsorption, increasing capacity.

Based on these data, we can conclude that the pitch coating contributes to cycling in a Si/pitch electrode. FTIR data showed that in the unannealed electrodes, the pitch does not completely cover the Si particles, so there is likely direct Si-Li alloying occurring in this sample. In the Si/pitch-700 sample, capacity increases compared to the pitch-700 electrode, both due to the addition of Si and due to the change of the carbon structure (Figs. 3c and 3d). The Si/pitch-1000 sample, however, has the lowest capacity of the Si/pitch set, likely due to the SiC observed with FTIR. The SiC

formed has lower electronic conductivity and appears to limit ionic conduction as well, effectively passivating any underlying Si and severely decreasing capacity.

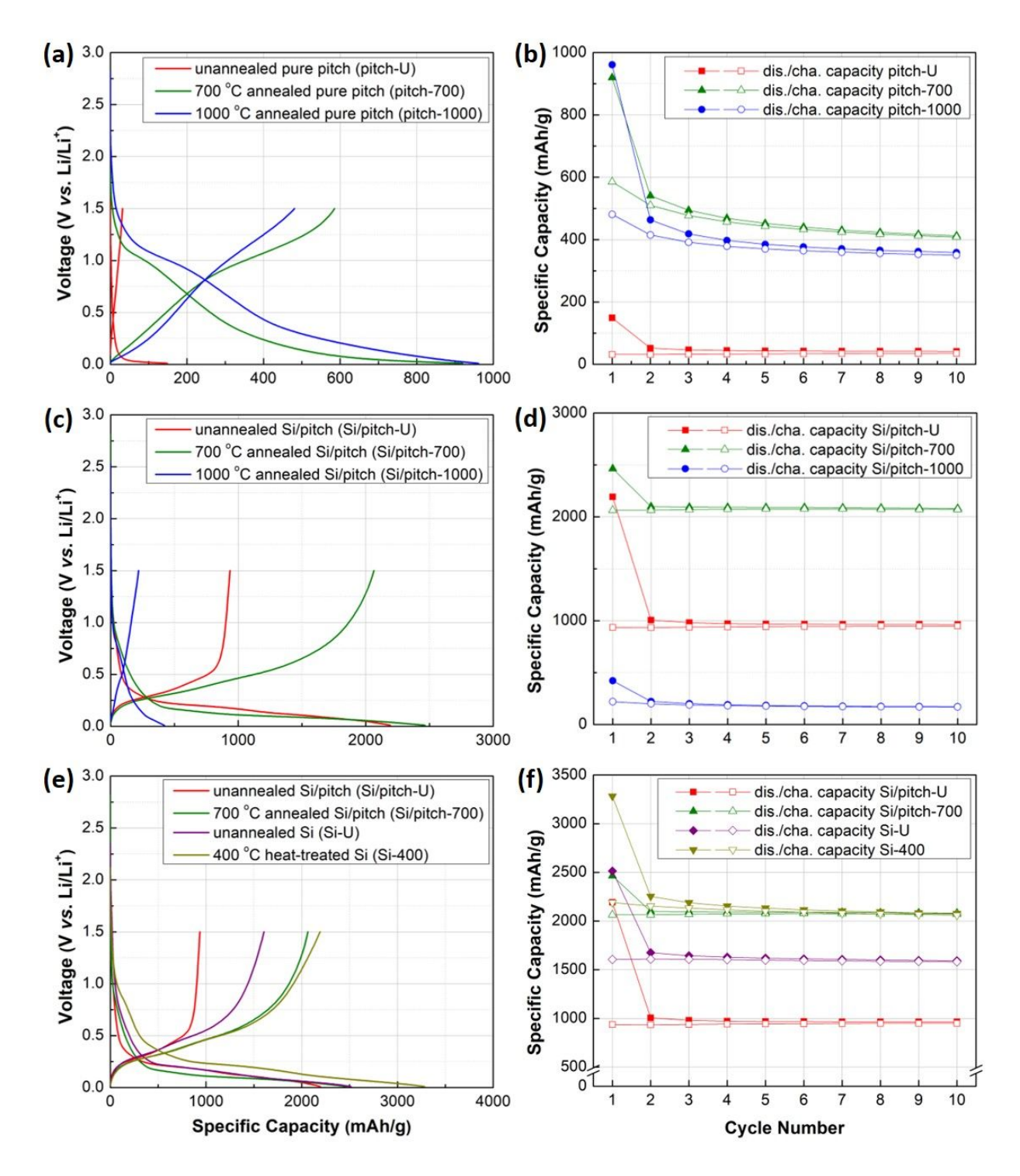


Figure 3. Voltage *vs.* specific capacity profiles and cycling performance of (a) and (b) pure pitch, (c) and (d) Si/pitch and (e) and (f) Si electrodes upon thermal annealing.

Electrodes made from PECVD silicon with NMP molecular surface functionalization were analyzed as well to better understand the role of the Si (Figs. 3e and 3f) [22]. One sample was heat-treated at 400 °C before cycling which removes the surface molecules, and one was cycled as is. The heat-treated Si electrode (Si-400) exhibited higher capacity than the non-heat treated one (Si-U). Our characterization showed no chemical or physical changes in these electrodes after heat treatment. Based on other studies, this capacity increase is likely due to the polymerization of the P84 polyimide binder that is used in these electrodes and the removal of surface molecules promoting improved porosity and ionic transport, rather than any changes in the Si [18, 40]. The heat-treated Si has a higher initial capacity than the Si/pitch-700; however, the Si/pitch-700 has an initial Coulombic efficiency (ICE) of 83.8%, while the heat-treated Si has an ICE of only 42.7%, as summarized in Table 1. While the ICE of the Si/pitch-700 is lower than the Si only, by the tenth cycle the Si/pitch-700 has a CE of 99.5%, while the Si only sample is 98.5%. It is known that, compared to graphite electrodes, Si electrodes experience significant parasitic reactions resulting in capacity fade due to their unstable SEI [41]. Because the pitch covers the Si in the 700 °C sample, these parasitic reactions are somewhat limited, indicating that it will likely perform better than the Si only sample over a higher number of cycles and that the pitch may help stabilize the SEI.

Table 1. Coulombic efficiency of Si/pitch and Si electrodes upon cycling.

Coulombic efficiency	(%))
----------------------	-----	---

	1 st cycle	2 nd cycle	10th cycle
Si/pitch-U	42.7	92.9	98.5
Si/pitch-700	83.8	98.3	99.5
Si/pitch-1000	52.2	90.0	98.4
Si-U	63.9	96.0	99.3
Si-400	66.8	95.6	99.2

Based on the cycling data of pitch-only, Si-only, and Si/pitch electrodes annealed and heat-treated at different temperatures, the pitch and Si both contribute to the cell performance. Additionally, annealing the powder of pitch-coated Si at 700 °C and heat treating the electrode at 400 °C are the optimal processing steps for this electrode system.

2.3. Aging behaviors of Si/pitch electrodes

2.3.1. SEI formation and evolution

A comparison of FTIR data from all Si/pitch electrodes cycled for 10 cycles was conducted to analyze the SEI species that formed, as shown in Figs. 4a-c. The Si/pitch-U showed evidence of known SEI species (e.g., lithium carbonate, lithium alkyl carbonate), while the peaks identified as Si and P84 binder were not present. The Si/pitch-700 sample showed similar SEI species as the unannealed sample, with the addition of polycarbonate, and with no clear P84 or Si peaks. Specifically, the FTIR spectra shows signals of a more polymeric SEI, i.e. poly-VC species, which have been shown to provide better cycling performance [42, 43]. The Si/pitch-1000 sample showed less signal from SEI species compared to the others, but some lithium carbonate was still observed. A clear SiC peak is observed, which is also observed on the pristine electrodes. The prominent SiC peak, observed both before and after cycling the Si/pitch-1000 sample, indicates the compound effectively passivates the surface prior to cycling [44, 45]. Based on this, we can conclude that the lower annealing temperature is necessary for optimal electrode performance.

Raman spectra of cycled electrodes at each annealing temperature was collected as well. The samples showed an increased FWHM as compared to their corresponding pristine samples (Figs. 1d-f), as seen in Figs. 4d-f and S5. While no SEI species are directly observed, the change in peak shape corresponds in a more amorphous structure and is likely due to SEI forming and obscuring

signal from the carbon. Additionally, increased background fluorescence seen in the cycled samples is likely due to SEI species.

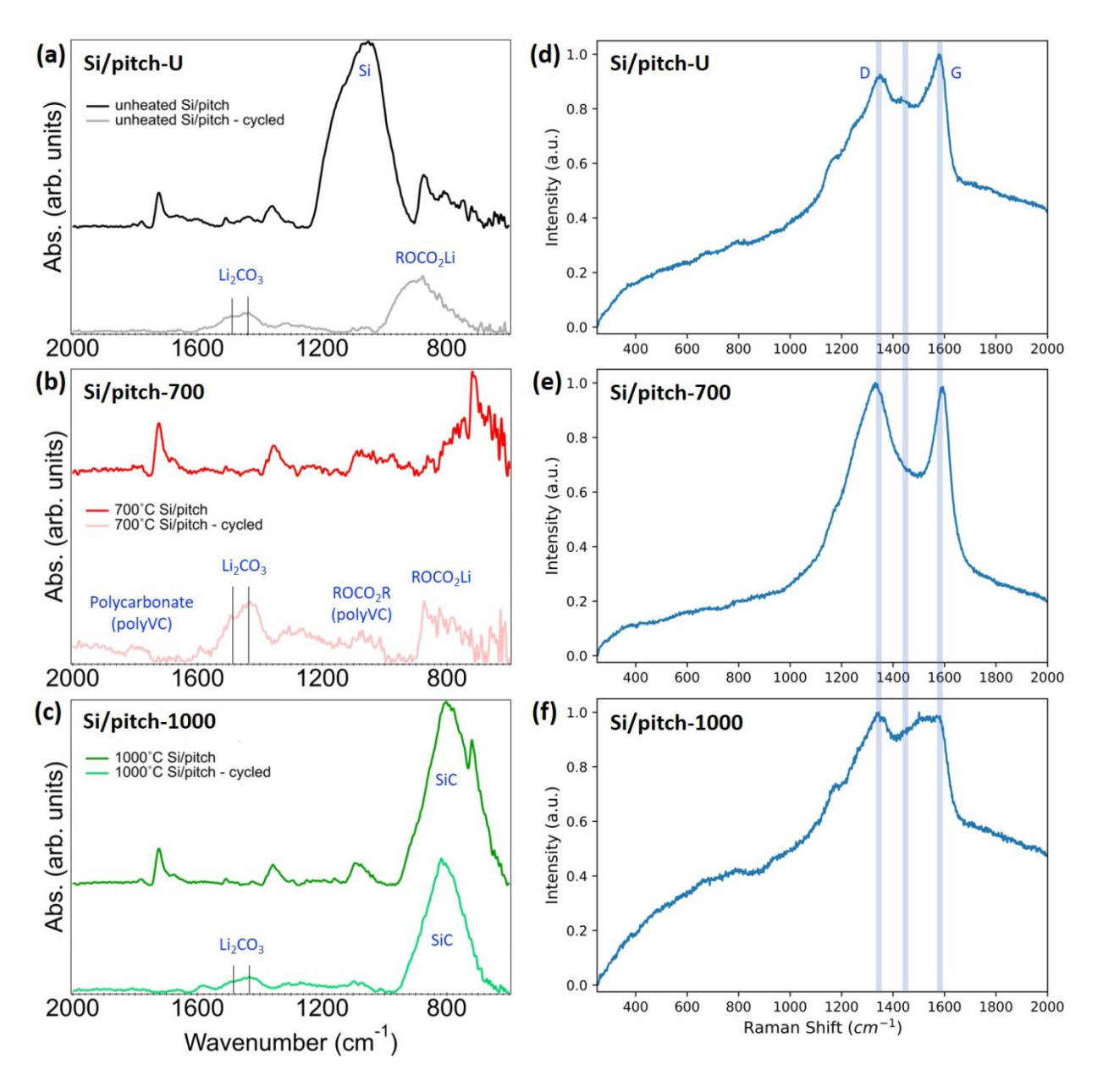


Figure 4. Surface chemistry changes of pristine *vs.* cycled (a) Si/pitch-U, (b) Si/pitch-700 and (c) Si/pitch-1000 electrodes. Raman spectra of cycled (d) Si/pitch-U, (e) Si/pitch-700 and (f) Si/pitch-1000 electrodes.

2.3.2. Heterogeneous aging behaviors

To better understand the surface chemistry changes on the electrodes, including SEI formation and evolution, structural changes, and possible ion storage behaviors of active materials during cycling, in-situ Raman spectra of Si/pitch-700 electrodes were collected for 10 cycles (Fig. S6). The newly developed in-situ vibrational spectroscopic technique based on our previous research demonstrate reproducible and reliable electrochemical performance over multiple cycles in terms of both electrochemistry and spectroscopy, which enables us to monitor the surface chemistry and structural changes of the electrode and to gain a fundamental and mechanistic understanding of the electrochemical behavior and performance of the cell [46].

Multiple measurements of Si/pitch-700 electrodes were analyzed and representative data is shown in Fig. 5. After the first cycle, we still observed a strong crystalline Si (c-Si) signal at around 520 cm⁻¹, as is seen in the pristine electrodes, indicating that little Li-Si alloying occurred. The signals from the carbon D and G bands are weaker during lithiation, but mostly recover during delithiation. It is possible this shift is due to the nature of the carbon active material changing and/or due to the presence of carbon-containing SEI species that cover the active material during lithiation and then are dissolved and/or separated during delithiation, re-exposing the underlying carbon. Specifically, a band that corresponds to Li₂CO₃, an SEI species formed from electrolyte decomposition and/or CO₂ or other impurities present within the cell, at 1475 cm⁻¹ is observed during both lithiation and delithiation for multiple cycles, indicating Li₂CO₃ could be a stable SEI species. After the fifth cycle, only amorphous silicon is seen, indicating that at this point, the Si has fully alloyed with the Li at this location on the sample. Additionally, an increasing peak FWHM of the carbon D and G bands throughout cycling indicates that more amorphous carbon is formed. There is still a change in the carbon character observed, similar to but less pronounced

than that seen in the first cycle. This change with increased cycling may indicate either a continual increase in SEI or a progressive change in the carbon as it stores ions, which may contribute to the lower ICE, as discussed previously.

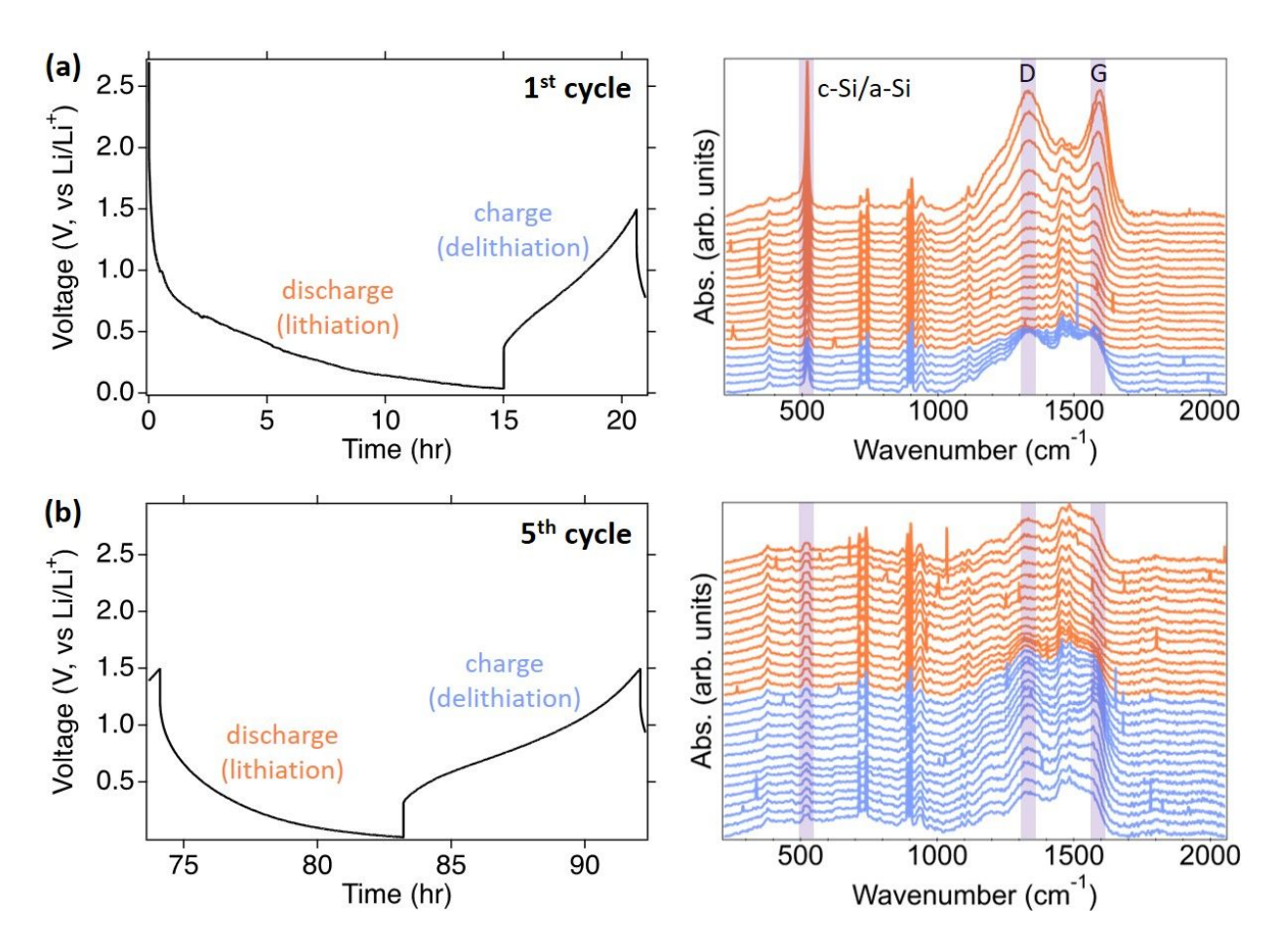


Figure 5. Time *vs.* voltage profiles and corresponding in-situ Raman spectra of the Si/pitch-700 electrodes for the (a) 1st and (b) 5th cycles.

After the 7th cycle in in-situ Raman, the microscope was moved to a new location on the electrode surface as shown schematically in Fig. 6. A weak c-Si and/or a-Si signal was observed during the 7th cycle (discharged at 70 mV), but a stronger one was seen during the 8th cycle (discharged at 70 mV) at the new location. These differences may be the result of heterogeneous cycling across the sample surface, where Si is being utilized for Li⁺ storage and changed into a-Si

in some places more than in others. Due to the nature of composite electrode and the mixing procedures used, the surface is not completely uniform, and the electrolyte encounters both the pitch-carbon and the Si, which both participate in ion storage. In some areas, the Si may be effectively blocked by the P84 polyimide binder used as well. There is some evidence that the P84 itself is (electro)chemically active, which could be an additional complicating factor [40, 47]. In the second location that is possibly covered with the binder, Li⁺ ion adsorption/desorption on the coated-pitch may be dominant with less reactions between Li⁺ ions and the underneath binder (Fig. 6a); whereas Li⁺ ion insertion/deinsertion into both the coated-pitch and underlying Li-Si alloy are dominant occurrences in the original location (Fig. 6b). Further study of this heterogeneous aging on the electrode surface using in-situ Raman mapping is a potential avenue for electrode optimization efforts by providing design guidance (e.g., surface modification of active materials and/or addition of surfactant(s)), as it is desirable to have as much Li⁺ stored in the Si as possible by homogeneous distribution of electrode components to achieve maximum capacity.

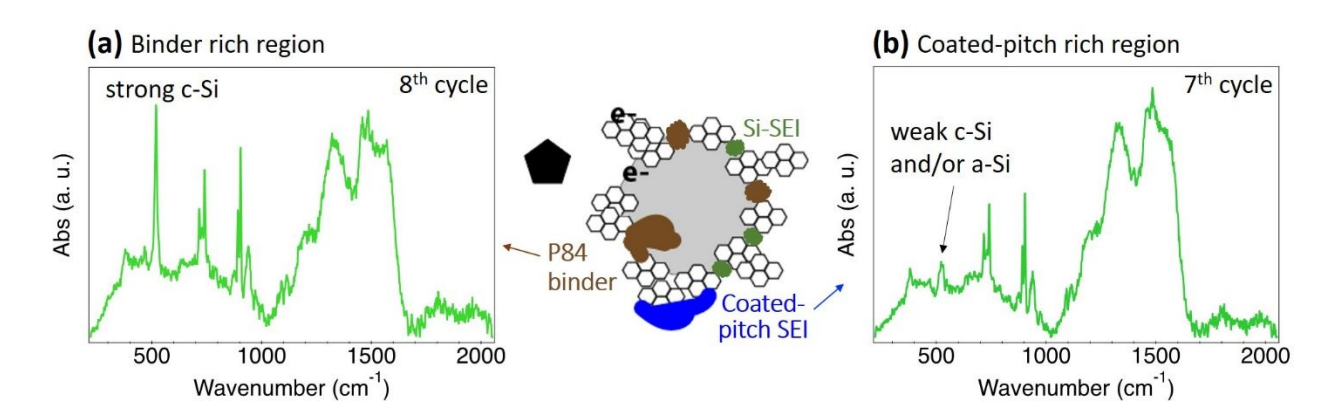


Figure 6. Heterogeneous aging behaviors of the Si/pitch-700 electrodes with different possible ion storage mechanisms and potential reactions for two different locations: (a) binder rich region and (b) coated-pitch rich region.

3. Conclusion

In this study, we present characterization of pitch-coated silicon electrodes, unannealed, annealed at 700 °C and at 1000 °C, before and after cycling. We demonstrate how 700 °C is the optimal annealing temperature for this system. It is shown that heat treatment altered the carbon structure prior to cycling and improved capacity during cycling. We also show how both the amorphous carbon/pitch and Si store Li⁺ions through different ion storage mechanisms (adsorption vs insertion) and contribute to overall performance through the study of pitch- and Si-only electrodes. This system showed an ICE of 83.8%, so future considerations should include efforts to improve this. Finally, we found that the electrodes underwent heterogeneous aging across the surface during cycling. Further study of this effect is required to understand its impact on long-term cycling and to make improvements if necessary.

4. Experimental Section

Preparation of Si/pitch electrodes and electrochemical cell tests. Full electrode synthesis and preparation details for the pitch-only and Si/pitch can be found in Schulze, et al [11]. The silicon-only electrode preparation is previously describes as well [18, 22]. The Gen2 electrolyte—1.2 M lithium hexafluorophosphate (LiPF₆) in ethylene carbonate (EC):ethyl methyl carbonate (EMC) (3:7 wt.%)—purchased from Tomiyama Pure Chemical Industries with 3 wt.% of fluoroethylene carbonate (FEC, Tomiyama Pure Chemical Industries) as an additive (GenF3) was used. Water contents of the electrolytes were measured using a Karl Fischer titrators (ETTLER TOLEDO C20S) located inside a glove box, and the values of all electrolytes were less than 10 ppm.

CR2032 coin-type cells were assembled in the Ar-filled glove box. The Si/pitch and pristine pitch electrodes (14 mm diameter), Li metal counter/reference electrodes (15 mm diameter),

separators (Celgard 2325, 19 mm diameter) and 40 μ L electrolyte were used to assemble the cells. All cells were tested in the MACCOR MTC-020 temperature chamber (at 25 °C) connected to a MACCOR Series 4000 Automated Test System. The cells were rested at open-circuit voltage (OCV) for 5 h before tests to ensure wetting of the electrodes. Galvanostatic discharge/charge tests were then performed in a range of 10 to 750 mV (vs. Li/Li⁺) at C/10 (1C corresponded to about 350 mA g⁻¹).

Characterization of Si/pitch electrodes. FTIR spectra were collected in attenuated total reflectance (ATR) mode using a Bruker Alpha II compact spectrometer and monolithic diamond ATR prism. The spectrometer is housed in an air-free argon gas filled glove box. Reference spectra were recorded against the argon background. Sample and background measurements consisted of an average of 192 scans. Spectra were baseline subtracted using a convex-hull baseline fit in Igor Pro data analysis software.

AFM and SSRM maps were collected using a Bruker Dimension Icon instrument installed in an Ar-filled glovebox to avoid air exposure. For AFM data, an Olympus AC160TS-R3 probe was used and for SSRM data, a conductive Bruker DDESP-V2 diamond coated probe. A -0.25 V bias was used to SSRM measurements. Images were processed using Bruker Nanoscope and Gwyddion software [30].

Time-resolved aging behavior analysis of Si/pitch electrodes. Si/pitch mesh electrodes were prepared under an inert argon atmosphere using conventional slurry formulation and casting techniques [11]. Typically, 8 mass equivalents of 700 °C annealed Si/pitch powder (Si:pitch = 50:50) were ball-milled (same parameters as before) with 1 mass equivalent of Timcal C65

conductive carbon. A 10 wt.% solution of P84 polyimide (Teacapowder P84, Ensinger Sintimid GmbH) in NMP was then added to the Si/pitch+carbon mixture in a screwcap scintillation vial such that the final slurry comprised 80:10:10 by mass of each the Si/pitch powder, Timcal C65, and P84 polyimide, respectively. Glass beads were added to the slurry, and the slurry was mixed with a Mazerustar KK-250S planetary mixer before being cast onto a Cu mesh current collector. The printed electrode was dried under vacuum at 150 °C for 4 hours, then underwent a subsequent 350 °C anneal for 4 h under 0.5 L/min of flowing nitrogen gas. Windowed coin-type cells were assembled using Si/pitch mesh electrodes (14 mm diameter) and Li metal counter/reference electrodes (15 mm diameter). The electrodes were separated by a 19 mm diameter circular punch of Celgard 2325, and 40 μL of GenF3 was added as the electrolyte.

In-situ Raman analysis was performed using a Bio-Logic SP-300 potentiostat/galavnostat. After 5 h rest at OCV the windowed coin-type cells were cycled between 0.01-1.5 V at C/10 (1C corresponding to 600 mAh/g). Either in-situ or ex-situ Raman spectra were measured using a confocal Horiba Xplora Plus Raman microscope with a 638 nm excitation source and a 50X-LWD (long working distance) objective lens with 1 percent laser power, 20 seconds exposure time and 30 accumulations. All measurement conditions were optimized to maximize the signal-to-noise ratio while minimizing possible beam damage [46].

Declaration of Competing Interests

The authors declare that they have no known competing financial interests or personal relationships that could have appeared to influence the work reported in this paper.

Acknowledgements

This work was supported by the faculty research fund of Sejong University in 2023. This work was authored by the National Renewable Energy Laboratory, operated by Alliance for Sustainable Energy, LLC, for the U.S. Department of Energy (DOE) under Contract No. DE-AC36-08GO28308. This research was supported by the U.S. Department of Energy's Vehicle Technologies Office under the Silicon Consortium Project, directed by Brian Cunningham, and managed by Anthony Burrell. The views expressed in the article do not necessarily represent the views of the DOE or the U.S. Government. The U.S. Government retains and the publisher, by accepting the article for publication, acknowledges that the U.S. Government retains a nonexclusive, paid-up, irrevocable, worldwide license to publish or reproduce the published form of this work, or allow others to do so, for U.S. Government purposes.

Credit Author Statement:

Zoey Huey: Validation, Formal analysis, Investigation, Data Curation, Writing - Original Draft.

Maxwell C. Schulze: Resources, Writing - Review & Editing. G. Michael Carroll: Resources,
Writing - Review & Editing. Chaiwat Engtrakul: Investigation, Data Curation, Writing - Original
Draft. Chun-Sheng Jiang: Funding acquisition. Steven C. DeCaluwe: Funding acquisition.

Bertrand J. Tremolet de Villers: Validation, Formal analysis, Investigation, Data Curation,
Writing - Original Draft, Writing - Review & Editing. Sang-Don Han: Conceptualization,

Methodology, Validation, Formal analysis, Investigation, Data Curation, Writing - Original Draft, Writing - Review & Editing, Supervision, Project administration, Funding acquisition.

References

- [1] M. N. Obrovac and L. J. Krause, Reversible Cycling of Crystalline Silicon Powder, *J. Electrochem. Soc.*, 2007, **154**(2), A103. DOI: 10.1149/1.2402112.
- [2] X. Su, Q. Wu, J. Li, X. Xiao, A. Lott, W. Lu, B. W. Sheldon and J. Wu, Silicon-Based Nanomaterials for Lithium-Ion Batteries: A Review, *Adv. Energy Mater.*, 2014, **4**(1), 1300882. https://doi.org/10.1002/aenm.201300882.
- [3] F. Ozanam and M. Rosso, Silicon as anode material for Li-ion batteries, *Mater. Sci. Eng., B.*, 2016, **213**, 2-11. https://doi.org/10.1016/j.mseb.2016.04.016.
- [4] E. Peled and S. Menkin, Review—SEI: Past, Present and Future, *J. Electrochem. Soc.*, 2017, **164**(7), A1703-A1719. DOI: 10.1149/2.1441707jes.
- [5] F. Wang, G. Chen, N. Zhang, X. Liu and R. Ma. Engineering of carbon and other protective coating layers for stabilizing silicon anode materials, *Carbon Energy*, 2019, **1**(2), 219-245. https://doi.org/10.1002/cey2.24.
- [6] M. Yoshio, H. Wang, K. Fukuda, T. Umeno, N. Dimov and Z. Ogumi, Carbon-Coated Si as a Lithium-Ion Battery Anode Material, *J. Electrochem. Soc.*, 2002, **149**(12), A1598-A1603. DOI: 10.1149/1.1518988.
- [7] K. Xu, X. Liu, K. Guan, Y. Yu, W. Lei, S. Zhang, Q. Jia and H. Zhang, Research Progress on Coating Structure of Silicon Anode Materials for Lithium-Ion Batteries, *ChemSusChem*, 2021, 14(23), 5135-5160. https://doi.org/10.1002/cssc.202101837.
- [8] S. Casino, P. Niehoff, M. Börner and M. Winter, Protective coatings on silicon particles and their effect on energy density and specific energy in lithium ion battery cells: A model study, *J. Energy Storage*, 2020, **29**, 101376. https://doi.org/10.1016/j.est.2020.101376.
- [9] Y.-X. Wang, S.-L. Chou, J. H. Kim, H.-K. Liu and S.-X. Dou. Nanocomposites of silicon and carbon derived from coal tar pitch: Cheap anode materials for lithium-ion batteries with long cycle life and enhanced capacity, *Electrochim. Acta*, 2013, **93**, 213-221. https://doi.org/10.1016/j.electacta.2013.01.092.
- [10] A. M. Escamilla-Pérez, A. Roland, S. Giraud, C. Guiraud, H. Virieux, K. Demoulin, Y. Oudart, N. Louvain and L. Monconduit, Pitch-based carbon/nano-silicon composite, an efficient anode for Li-ion batteries, *RSC Adv.*, 2019, **9**(19), 10546-10553. https://doi.org/10.1039/C9RA00437H.
- [11] M. C. Schulze, K. Fink, J. Palmer, G. M. Carroll, N. S. Dutta, C. Zwiefel, C. Engtrakul, S.-D. Han, N. R. Neale and B. J. Tremolet de Villers, Pitch Carbon-coated Ultrasmall Si Nanoparticle Lithium-ion Battery Anodes Exhibiting Reduced Reactivity with Carbonate-based Electrolyte, *Batter. Supercaps*, 2023, **6**(9), e202300186. https://doi.org/10.1002/batt.202300186. [12] P. Li, J.-Y. Hwang and Y.-K. Sun, Nano/Microstructured Silicon-Graphite Composite Anode for High-Energy-Density Li-Ion Battery, *ACS Nano*, 2019, **13**(2), 2624-2633.
- [13] Y. Nishi, The development of lithium ion secondary batteries, *Chem. Rec.*, 2001, **1**(5), 406-413. https://doi.org/10.1002/tcr.1024.
- [14] Y. Zhang, X. G. Zhang, H. L. Zhang, Z. G. Zhao, F. Li, C. Liu and H. M. Cheng, Composite anode material of silicon/graphite/carbon nanotubes for Li-ion batteries, *Electrochim. Acta.*, 2006, **51**(23), 4994-5000. https://doi.org/10.1016/j.electacta.2006.01.043.
- [15] J. R. Dahn, T. Zheng, Y. Liu and J. S. Xue, Mechanisms for Lithium Insertion in Carbonaceous Materials, *Science*, 1995, **270**(5236), 590-593. DOI: 10.1126/science.270.5236.590.

https://doi.org/10.1021/acsnano.9b00169.

- [16] N. A. Kaskhedikar and J. Maier, Lithium Storage in Carbon Nanostructures, *Adv. Mater.*, 2009, **21**(25-26), 2664-2680. https://doi.org/10.1002/adma.200901079.
- [17] B. Babu, P. Simon and A. Balducci, Fast Charging Materials for High Power Applications, *Adv. Energy Mater.*, 2020, **10**(29), 2001128. https://doi.org/10.1002/aenm.202001128.
- [18] M. C. Schulze, F. Urias, N. S. Dutta, Z. Huey, J. Coyle, G. Teeter, R. Doeren, B. J. Tremolet de Villers, S.-D. Han, N. R. Neale and G. M. Carroll, Control of nanoparticle dispersion, SEI composition, and electrode morphology enables long cycle life in high silicon content nanoparticle-based composite anodes for lithium-ion batteries, *J. Mater. Chem. A.*, 2023, 11(10), 5257-5266, https://doi.org/10.1039/D2TA08935A.
- [19] B. Apicella, A. Tregrossi, F. Stazione, A. Ciajolo and C. Russo, Analysis of Petroleum and Coal Tar Pitches as Large PAH, *Chem. Eng. Trans.*, 2017, **57**, 775-780. DOI: 10.3303/CET1757130.
- [20] G. M. Carroll, R. Limpens and N. R. Neale, Tuning Confinement in Colloidal Silicon Nanocrystals with Saturated Surface Ligands, *Nano Lett.*, 2018, **18**(5), 3118-3124. https://doi.org/10.1021/acs.nanolett.8b00680.
- [21] A. Kleinová, J. Huran, V. Sasinková, M. Perný, V. Šály and J. Packa, FTIR spectroscopy of silicon carbide thin films prepared by PECVD technology for solar cell application, Proc. SPIE 9563, Reliability of Photovoltaic Cells, Modules, Components, and Systems VIII, 95630U (23 September 2015). https://doi.org/10.1117/12.2186748.
- [22] G. M. Carroll, M. C. Schulze, T. R. Martin, G. F. Pach, J. E. Coyle, G. Teeter and N. R. Neale, SiO₂ Is Wasted Space in Single-Nanometer-Scale Silicon Nanoparticle-Based Composite Anodes for Li-Ion Electrochemical Energy Storage, *ACS Appl. Energy Mater.*, 2020, **3**(11), 10993–11001. https://doi.org/10.1021/acsaem.0c01934.
- [23] A. Fakhri, S. Rashidi, M. Asif and A. A. Ibrahim, Microwave-Assisted Synthesis of SiC Nanoparticles for the Efficient Adsorptive Removal of Nitroimidazole Antibiotics from Aqueous Solution, *Appl. Sci.*, 2017, 7(2), 205. https://doi.org/10.3390/app7020205.
- [24] I. H. Son, J. H. Park, S. Kwon, S. Park, M. H. Rümmeli, A. Bachmatiuk, H. J. Song, J. Ku, J. W. Choi, J. Choi, S.-G. Doo and H. Chang, Silicon carbide-free graphene growth on silicon for lithium-ion battery with high volumetric energy density, *Nat. Commun.*, 2015, **6**, 7393. https://doi.org/10.1038/ncomms8393.
- [25] C. Yu, X. Chen, Z. Xiao, C. Lei, C. Zhang, X. Lin, B. Shen, R. Zhang and F. Wei, Silicon Carbide as a Protective Layer to Stabilize Si-Based Anodes by Inhibiting Chemical Reactions, *Nano Lett.*, 2019, **19**(8), 5124-5132. https://doi.org/10.1021/acs.nanolett.9b01492.
- [26] M. Dumont, G. Chollon, M. A. Dourges, R. Pailler, X. Bourrat, R. Naslain, J. L Bruneel and M. Couzi, Chemical, microstructural and thermal analyses of a naphthalene-derived mesophase pitch, *Carbon*, 2002, **40**(9), 1475-1486. https://doi.org/10.1016/S0008-6223(01)00320-7.
- [27] D. B. Schuepfer, F. Badaczewski, J. M. Guerra-Castro, D. M. Hofmann, C. Heiliger, B. Smarsly and P. J. Klar, Assessing the structural properties of graphitic and non-graphitic carbons by Raman spectroscopy, *Carbon*, 2020, **161**, 359-372. https://doi.org/10.1016/j.carbon.2019.12.094.
- [28] Z. Li, L. Deng, I. A. Kinloch and R. J. Young, Raman spectroscopy of carbon materials and their composites: Graphene, nanotubes and fibres, *Prog. Mater Sci.*, 2023, **135**, 101089. https://doi.org/10.1016/j.pmatsci.2023.101089.
- [29] C. Stetson, T. Yoon, J. Coyle, W. Nemeth, M. Young, A. Norman, S. Pylypenko, C. Ban, C.-S. Jiang, M. Al-Jassim and A. Burrell, Three-dimensional electronic resistivity mapping of

- solid electrolyte interphase on Si anode materials, *Nano Energy*, 2019, **55**, 477-485. https://doi.org/10.1016/j.nanoen.2018.11.007.
- [30] Z. Huey, Y. Ha, S. Frisco, A. Norman, G. Teeter, C.-S. Jiang and S. C. DeCaluwe, Multi-modal characterization methods of solid-electrolyte interphase in silicon-graphite composite electrodes, *J. Power Sources*, 2023, **564**, 232804.
- https://doi.org/10.1016/j.jpowsour.2023.232804.
- [31] P. Eyben, W. Vandervorst, D. Alvarez, M. Xu and M. Fouchier, Probing Semiconductor Technology and Devices with Scanning Spreading Resistance Microscopy, New York, NY, Springer New York, 2007, 31-87.
- [32] C. Stetson, Z. Huey, A. Downard, Z. Li, B. To, A. Zakutayev, C.-S. Jiang, M. M. Al-Jassim, D. P. Finegan, S.-D. Han and S. C. DeCaluwe, Three-Dimensional Mapping of Resistivity and Microstructure of Composite Electrodes for Lithium-Ion Batteries, *Nano Lett.*, 2020, **20**(11), 8081-8088. https://doi.org/10.1021/acs.nanolett.0c03074.
- [33] A. G. Pandolfo and A. F. Hollenkamp, Carbon properties and their role in supercapacitors, *J. Power Sources*, 2006, **157**(1), 11-27. https://doi.org/10.1016/j.jpowsour.2006.02.065.
- [34] Y. Li, L. Mu, Y.-S. Hu, H. Li, L. Chen and X. Huang, Pitch-derived amorphous carbon as high performance anode for sodium-ion batteries, *Energy Storage Mater.*, 2016, **2**, 139-145. https://doi.org/10.1016/j.ensm.2015.10.003.
- [35] F. G. Emmerich, Young's modulus, thermal conductivity, electrical resistivity and coefficient of thermal expansion of mesophase pitch-based carbon fibers, *Carbon*, 2014, **79**, 274-93. https://doi.org/10.1016/j.carbon.2014.07.068.
- [36] T. Nakazawa, K. Oshida, N. Ono, K. Ohsawa, M. Endo and S. Bonnamy, Structure and electrical resistivity of nano-carbon materials, *Thin Solid Films*, 2004, **464-465**, 360-363. https://doi.org/10.1016/j.tsf.2004.06.034.
- [37] K. J. Kim, K.-Y. Lim, Y.-W. Kim and H. C. Kim, Temperature Dependence of Electrical Resistivity (4-300 K) in Aluminum- and Boron-Doped SiC Ceramics, *J. Am. Ceram. Soc.*, 2013, **96**(8), 2525-2530. https://doi.org/10.1111/jace.12351.
- [38] W.-R. Liu, Z.-Z. Guo, W.-S. Young, D.-T. Shieh, H.-C. Wu, M.-H. Yang and N.-L. Wu, Effect of electrode structure on performance of Si anode in Li-ion batteries: Si particle size and conductive additive, *J. Power Sources*, 2005, **140**, 139–144. https://doi.org/10.1016/j.jpowsour.2004.07.032.
- [39] J. H. Kim, Z. Huey, G. M. Veith, C.-S. Jiang, N. R. Neale and G. M. Carroll, Blended 1D carbon nanostructures synergistically enhance electron and ion transport in silicon nanoparticle electrodes, *Cell Rep. Phys. Sci.*, 2024, **5**(6), 101974. https://doi.org/10.1016/j.xcrp.2024.101974. [40] S. Rajendran, H. Liu, S. E. Trask, B. Key, A. N. Jansen and M.-T. F. Rodrigues,
- Consequences of utilizing a redox-active polymeric binder in Li-ion batteries, *J. Power Sources*, 2023, **583**, 233584. https://doi.org/10.1016/j.jpowsour.2023.233584.
- [41] F. Holtstiege, A. Wilken, M. Winter and T. Placke, Running out of lithium? A route to differentiate between capacity losses and active lithium losses in lithium-ion batteries, *Phys. Chem. Chem. Phys.*, 2017, **19**(38), 25905-25918. https://doi.org/10.1039/C7CP05405J.
- [42] A. L. Michan, B. S. Parimalam, M. Leskes, R. N. Kerber, T. Yoon, C. P. Grey and B. L. Lucht, Fluoroethylene Carbonate and Vinylene Carbonate Reduction: Understanding Lithium-Ion Battery Electrolyte Additives and Solid Electrolyte Interphase Formation, *Chem. Mater.*, 2016, **28**(22), 8149-8159. DOI: 10.1021/acs.chemmater.6b02282.
- [43] Y. Jin, N.-J. H. Kneusels, P. C. M. M. Magusin, G. Kim, E. Castillo-Martínez, L. E. Marbella, R. N. Kerber, D. J. Howe, S. Paul, T. Liu and C. P. Grey, Identifying the Structural

- Basis for the Increased Stability of the Solid Electrolyte Interphase Formed on Silicon with the Additive Fluoroethylene Carbonate, *J. Am. Chem. Soc.*, 2017, **139**(42), 14992-15004. DOI: 10.1021/jacs.7b06834.
- [44] M. S. Anwar, S. Z. A. Bukhari, J.-H. Ha, J. Lee, I.-H. Song and Y.-W. Kim, Controlling the electrical resistivity of porous silicon carbide ceramics and their applications: A review, *Int. J. Appl. Ceram.*, 2022, **19**(4), 1814-1840. https://doi.org/10.1111/ijac.14034.
- [45] A. Timmons, A. D. W. Todd, S. D. Mead, G. H. Carey, R. J. Sanderson, R. E. Mar and J. R. Dahn, Studies of $Si_{1-x}C_x$ Electrode Materials Prepared by High-Energy Mechanical Milling and Combinatorial Sputter Deposition, *J. Electrochem. Soc.*, 2007, **154**(9), A865-A874. DOI: 10.1149/1.2755782.
- [46] Y. Ha, B. J. Tremolet de Villers, Z. Li, Y. Xu, P. Stradins, A. Zakutayev, A. Burrell and S.-D. Han, Probing the Evolution of Surface Chemistry at the Silicon-Electrolyte Interphase via In Situ Surface-Enhanced Raman Spectroscopy, *J. Phys. Chem. Lett.* 2020, **11**(1), 286-291. https://doi.org/10.1021/acs.jpclett.9b03284.
- [47] B. N. Wilkes, Z. L. Brown, L. J. Krause, M. Triemert and M. N. Obrovac, The Electrochemical Behavior of Polyimide Binders in Li and Na Cells, *J. Electrochem. Soc.*, 2016, **163**(3), A364-A372. DOI: 10.1149/2.0061603jes.

The data supporting this article have been included as part of the Supplementary Information.